

# Dispersion of waves in piano strings

Michael Podlesak and Anthony R. Lee

Physics Department, La Trobe University, Bundoora, Victoria 3083, Australia

(Received 18 April 1986; accepted for publication 20 August 1987)

A recent survey of piano acoustics literature revealed an apparent lack of attention to various aspects of dispersion in piano strings, apart from some information on its effect on inharmonicity of piano tone partials. In this article, it will be shown how group velocity of transverse waves in piano strings can be measured as a function of frequency with the aid of a short-time spectral analysis method. Examples of group velocity measurements appear to be essentially in agreement with the theoretical predictions based on a model of a flexurally stiff string. In addition, the relationship between the group and phase velocity, as a function of frequency, is also illustrated, indicating correspondence between theoretical predictions and experimental results. A short-time spectral analysis of transverse string displacement as a function of time, monitored near the bridge, has revealed a quasiperiodic succession of frequency glides. This effect is due to dispersion and is particularly prominent in the lowest bass strings. However, the same type of analysis applied to the sound-pressure signal of the corresponding radiated sound yielded somewhat different results. While frequency glides similar to those found in the string displacement spectra were partly evident in the sound-pressure spectra, strong precursive components of longitudinal string vibration origin were found to dominate the higher frequency portion of the attack transient of the radiated sound.

PACS numbers: 43.75.Mn

## INTRODUCTION

Wave dispersion is a commonly observed phenomenon and occurs in media that transmit harmonic waves of differing frequencies at different speeds. It can be said that a piano string constitutes a one-dimensional linear dispersive medium due to its bending stiffness. The effect of dispersion in piano strings is clearly manifested by the inharmonicity<sup>1-6</sup> of piano tones. However, it appears that, so far, no group velocity measurements of transverse waves in piano strings have been attempted nor has the study of the possible effects that dispersion may have on the attack transients of piano tones.

Our initial observations of displacement variation in time of a bass string, monitored near the bridge, displayed a strong presence of dispersion through the appearance of low-amplitude precursors (see Fig. 1). In general, a complex traveling wave propagating in a linear, dispersive medium will not retain a constant shape even if the attenuation is minimal. Baldock and Bridgeman<sup>7</sup> have shown that, for a traveling wave train in a dispersive medium, the main body travels at group velocity preceded by low-amplitude precursors. These precursors, in the case of the piano string, vibrate at a greater rate than the main body of the wave train. An analogous effect can be clearly observed on the  $A_0$  (27.5-Hz) string, as shown in Fig. 1, although, due to reflection at the string boundaries, the process is not the same as for a traveling wave group on an infinitely long string. It can be shown, however, by use of elementary considerations similar to Johns,<sup>8</sup> that the more rapidly vibrating precursors will be sufficiently advanced from the main body of the group, to display a comparable behavior for at least one or two periods. This effect is most evident in the lowest bass strings on account of the large number of significant partials present in the initial portion of the attack transient, combined with substantial flexural stiffness of the string.

A more quantitative assessment of the effects of dispersion, besides inharmonicity of string vibration partials, such as group velocity variation with frequency, required the application of a short-time spectral analysis technique, described in Sec. II. This technique was also employed to investigate the correlation between the attack transient of the transverse string vibration spectra and the sound-pressure spectra of the corresponding radiated sound.

## I. THEORY

All piano bass strings are characterized by a steel core wire wrapped with copper or, sometimes, iron windings, used to increase the string's linear mass density. While the tight coiling on the copper wire ensures close coupling to the

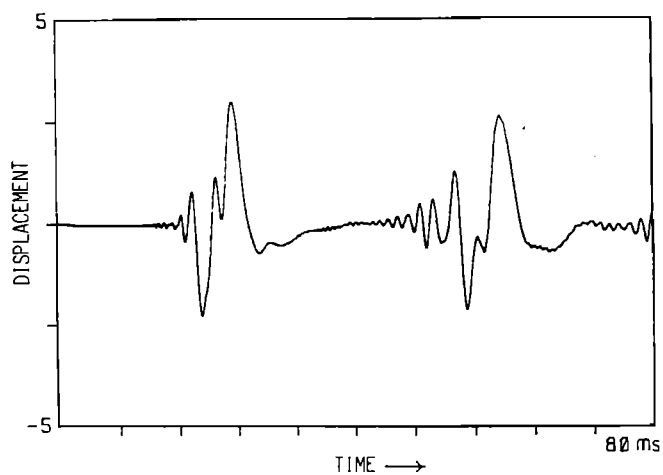


FIG. 1. A trace of the perpendicular-to-soundboard displacement of the  $A_0$  (27.5-Hz) string in time, showing the first two initial pulses monitored near the bridge. The displacement scale units are arbitrary.

core, the windings contribute considerably more to the increase in the string's linear mass density than to its bending stiffness. In a real piano bass string, the copper windings do not extend over the string's supports, but end just short of the agraffe and the bridge, leaving two very short lengths of bare, exposed steel core.

In order to demonstrate the effects of the physical phenomenon of dispersion, it will suffice to assume a simplified model of the piano string with uniform linear mass density and with ends pinned to two rigid and massive supports. The latter assumption will be slightly relaxed when considering radiated sound, as some vibrational energy must be transmitted to the soundboard through the bridge. However, within the scope of our group velocity measurements of transverse waves in the string, the ensuing changes in the frequency of partials due to the movement of the bridge are not expected to affect our results to any significant degree.

The dispersion relation for transverse waves on a uniform piano string with circular cross section and flexural stiffness is given here by

$$YS^2k^4/(4\pi\sigma) + Tk^2/\sigma = \omega^2, \quad (1)$$

where  $k$  is the wavenumber,  $\omega$  is the angular frequency,  $Y$  is the Young's modulus of elasticity,  $T$  is the string tension,  $S$  is the cross-sectional area of the steel core, and  $\sigma$  is the linear mass density of the string. In Ref. 2, for example, this equation is derived for a plain string in slightly different terms; namely,  $T\mu^2 + 4\pi^2QS\kappa^2\mu^4 = \rho S\nu^2$ , where, in comparison with Eq. (1),  $T = T$ ,  $Q = Y$ ,  $\mu = k/2\pi$ , and  $\nu = \omega/2\pi$ . Here,  $\rho S$  ( $\rho$  being the volume density of the plain string) is replaced by  $\sigma$ , since the string's cross section relevant to stiffness calculations is essentially that due to the steel core and not the windings. The  $\kappa$  is the radius of gyration, with  $\kappa^2 = S/4\pi$  for a circular cross section of the steel core.

In a one-dimensional, linear, and homogeneous medium, standard wave theory (e.g., Ref. 7) defines phase and group velocities  $v_p$  and  $v_g$  as

$$v_p = \omega/k \quad (2)$$

and

$$v_g = \frac{\partial\omega}{\partial k}, \quad (3)$$

which we set out in here for reference. From these definitions, it can be shown that the relationship between  $v_g$  and  $v_p$ , based on the dispersion relation (1), can be expressed by

$$v_g = (2v_p - c_0^2/v_p), \quad (4)$$

with  $c_0^2 = T/\sigma$ . This relation can be gainfully applied in the comparison of measured values of  $v_g$  and  $v_p$  without the knowledge of the string's particular physical parameters.

However,  $v_p$  and  $v_g$  can be expressed as functions of frequency ( $\nu = \omega/2\pi$ ), by substituting Eq. (1) into Eqs. (2) and (3), respectively, and by solving Eq. (1) for  $k$  in terms of  $\omega$ . We obtain

$$v_p = \{(T/2\sigma + [(T/2\sigma)^2 + YS^2\pi\nu^2/\sigma]^{1/2})\}^{1/2} \quad (5)$$

and

$$v_g = [(T/\sigma)^2 + 4YS^2\pi\nu^2/\sigma]^{1/2}\{T/2\sigma + [(T/2\sigma)^2 + YS^2\pi\nu^2/\sigma]^{1/2}\}^{-1/2}. \quad (6)$$

In our investigations, we have used Eqs. (5) and (6) to predict the group and phase velocity of transverse waves as functions of frequency in three representative examples of piano strings.

## II. EXPERIMENTAL METHOD AND APPARATUS

Our experiments were carried out on a 6-f Yamaha model G3 grand piano, serial number E 1863412. A photovoltaic detector<sup>9</sup> used to monitor the relative displacement of a given piano string was placed over the string, usually near one of the end supports. Although the device is capable of monitoring independently two components of the string's transverse vibration at a single point, only the more significant (perpendicular-to-soundboard) component<sup>10,11</sup> was considered in our present analysis. Only single tones were investigated.

The string displacement signals were recorded on a Revox B77 MK II two-track audio tape recorder. The corresponding sound-pressure variations of radiated sound were recorded via two type 4145 Brüel & Kjaer 1-in. microphones, coupled to two type 2639 preamplifiers, energized by a type 2804 dual power supply. The microphone output signals were recorded on a Grundig TS-1000 four-track audio tape recorder. The recorded photovoltaic and microphone signals were subsequently analyzed on an Ono Sokki CF-300 FFT analyzer, coupled to an Ono Sokki CX-337 color plotter.

In our experiments, the piano was situated at one end of a sound recording studio with a rectangular floor plan, approximately  $4 \times 12$  m, and a ceiling height of 2.5 m. Most of the studio's surfaces were covered with soft furnishings that reduced the room's reverberation time. Of the two microphones used, one was placed 10 cm above the central portion of the piano soundboard (see Fig. 2) and the other about 2 m away from the piano, facing the keyboard player at a 45-degree angle on the right-hand side. The vertical elevation of the second microphone was approximately 1.6 m above the studio floor. Figure 2 shows the piano lid in a vertical position, which is rather unusual for most musical performances. However, the lid had to be raised sufficiently to accommodate the prototype of the string vibration pickup, placed on a board supported by the rim of the piano case. Although such an experimental arrangement may not be the most satisfactory one from a musical point of view, it was considered quite adequate for the purpose of our investigation.

The Ono Sokki CF-300 FFT (fast Fourier transform) portable analyzer was used for all frequency and time-domain measurements. It covers the frequency range from 0 to 20 kHz, with a sampling frequency of 51.2 kHz for the largest signal frequency range, and is equipped with a 120-dB/oct digital antialiasing filter. The analyzer has a maximum dynamic range of 72 dB and it produces spectra from 512 sample points of captured data with resolution of 200 points over any given frequency-range setting in the nonzoom mode. The windowing function employed in most analyses was of the Hanning type. It is understood that accurate spectral levels of short transient signals cannot be obtained by use



FIG. 2. An example of the experimental arrangement on the Yamaha model G3 grand piano.

of the Hanning window. In most cases of frequency analysis in our investigations, however, such accuracy was not required. The aggregate frequency response of the measurement and analysis equipment was 20 Hz to 20 kHz.

From Fourier transform theory, it is well known<sup>2,7,12</sup> that the relationship between the frequency and time resolution of an observed sinusoidal signal is

$$\Delta f \Delta T \sim 1, \quad (7)$$

where  $\Delta f$  and  $\Delta T$  are measures of frequency and time spread, respectively. This means that the greater the length of the time signal analyzed, the more accurately one can determine the corresponding frequency spectrum.<sup>13</sup> In our experiments on the piano, both long- and short-time record analysis techniques were used. Since most of the signals analyzed changed relatively slowly in amplitude and frequency after the attack, it was possible to obtain highly resolved spectra of the signal eigenfrequencies for sufficiently long time-record lengths. The spectra resembled somewhat the Fourier series type of result because of their discrete and almost periodic distribution of amplitude peaks in frequency. For time-record length comparable to, or smaller than, the string's fundamental period of vibration, the frequency components were poorly resolved. As expected, for signal samples of short duration, the frequency spectra were of a continuous appearance, but the time development was better defined as implied by Eq. (7).

In the particular case of standing wave modes on the

piano string, the short-time frequency analysis of transverse string displacement signal can be exploited to calculate group velocity as a function of frequency. By selecting a particular frequency band on the FFT analyzer, with central frequency  $\nu$ , one obtains a plot of displacement level as a function of time, which, in principle, is similar to the autocorrelation function of the frequency group contained within the bandwidth of the analysis channel,  $\nu \pm \Delta\nu/2$ . The periodicity  $T(\nu)$  of the ensuing peaks (see, for example, Fig. 5) is related to the velocity of the group  $v_g$  and the length of the group's to-and-fro journey along the string  $2L$ . Thus an estimate of the group velocity  $v_g(\nu)$  of transverse waves on the string may be obtained from

$$v_g(\nu) = 2L/T(\nu). \quad (8)$$

While an accurate displacement level may not be indicated when the Hanning window is used, which is necessary to avoid spurious components due to the spectral leakage when a rectangular window is used, the period  $T$  should not be significantly affected as long as the observed group remains reasonably coherent over a period of one round-trip journey of the pulse.

In most of our group velocity measurements, the photovoltaic detector was placed near the bridge, but not too close in order to diminish components arising from the bridge motion. Measurements were taken for single piano tones played forte, with the string vibrations allowed to decay freely. Analysis ranges of 5, 10, and 20 kHz were used, with the

corresponding sampling rate of the FFT analyzer set at 12.8, 25.6, and 51.2 kHz, respectively. These, in turn, set the respective window lengths to 40, 20, and 10 ms and the channel bandwidths to 25, 50, and 100 Hz. The sampling overlap was adjustable, but, for most group velocity measurements, it was set to 6.25%. In some instances, the time differentiating option within the FFT analyzer was used to enhance the spectral amplitudes in the high-frequency portion of the string displacement spectra. In this way, a  $2\pi\nu$  factor was introduced into the amplitude of the analyzed signal.

The recorded displacement and sound-pressure signal levels referred to in the subsequent text and figures were not related to an absolute standard. While standardized measurements would be useful, they are not absolutely necessary in an initial study of this kind, which is primarily intended for the demonstration of the effects of the physical phenomenon of dispersion.

### III. RESULTS

An example of a short-time string vibration spectrum is given in Fig. 3, which shows a lobed distribution of the displacement level spectra for the  $A_0$  (27.5-Hz) string. The lobes are associated with the piano hammer's striking-distance to string-length ratio, and their width increases with frequency due to dispersion. The effect of the striking-distance to string-length ratio is more clearly illustrated in Fig. 4, which represents essentially the same spectrum as Fig. 3, but with the sampling rate decreased fivefold. The resultant spectrum assumes a discrete appearance and the spectral envelope minima appear between the 8th and the 9th partials, at the 17th partial, etc. Since the greatest inhibition of partials occurs in the hammer impact region, it is evident from Fig. 4 that it coincides approximately with a  $1/8.5$  striking-distance to string-length ratio. This, in turn, corresponds to a hammer striking distance of approximately 160 mm from the agraffe, which is reasonably consistent with the actual hammer-line measurement for the  $A_0$  string.

The highly regular fluctuations of displacement level in time of the  $A_0$  string, evident in Fig. 5, relate to the time periods of round-trip journeys of wave groups, with center frequencies indicated at the lower left portion of each indi-

vidual plot. Similar plots were obtained for the corresponding relative sound-pressure signal, shown in Fig. 6, after applying the same kind of analysis as for the string displacement signal. These also display identical fluctuations in terms of repetition rate. However, because of the complexity in the transmission path of the vibrational energy from the string to the monitoring microphone, as well as possible interference from other sound sources, group velocity measurements derived from sound-signal data cannot always be relied upon.

The regularity of the lobed pattern in the time plots of the string's displacement level for a particular frequency group, i.e., a wave packet with frequencies contained within the  $\nu \pm \Delta\nu/2$  band, can be exploited to increase the accuracy to which group velocity can be determined. This is achieved simply by taking the mean value of the round-trip time of the wave packet propagating along the string over a large number of periods. On applying Eq. (8) to data obtained from the time plots of  $A_0$  displacement level, the group velocity  $v_g(\nu)$  for a range of frequency channels  $\nu \pm 12.5$  Hz is calculated and listed in Table I.

Most of the values of  $\nu$  for which  $v_g$  has been calculated were chosen to correspond approximately to the central frequencies of each displacement level lobe, shown in Fig. 3. With displacement amplitude spectrum on a linear scale, these lobes resemble an amplitude distribution in frequency, which is characteristic of a Gaussian wave packet (e.g., Ref. 14). In fact, a closer examination of string displacement variation in time, shown in Fig. 1, reveals the presence of several individual wave packets, which are sufficiently separated from the main group to be distinctly identified. An estimate of their apparent frequency, which is roughly equivalent to the mean frequency of their quasi-Gaussian distribution,<sup>14</sup> can be shown to correspond to the appropriate central lobe frequencies in Fig. 3.

The group velocity measurement error increased with frequency, mainly because of the decreasing signal-to-noise

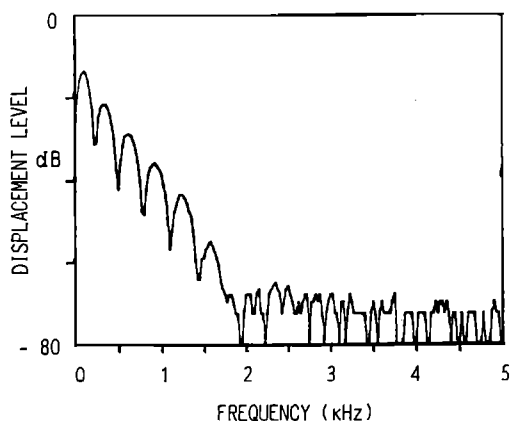


FIG. 3. The cumulative peak displacement level spectrum of the  $A_0$  (27.5-Hz) string vibration, monitored near the piano-bridge end. (Noise predominates in the 2-to-5-Hz region.)

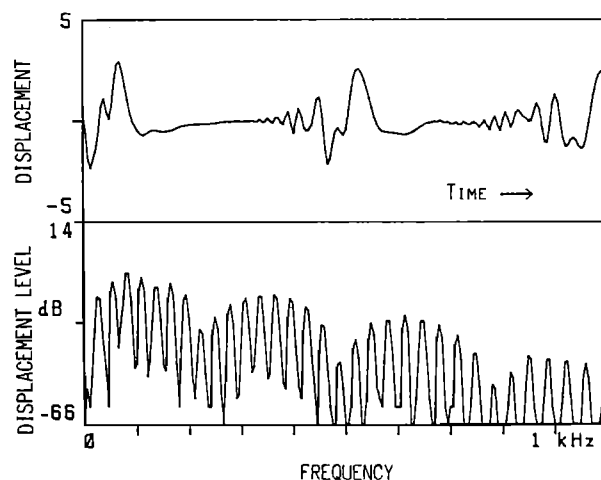


FIG. 4. The  $A_0$  (27.5-Hz) string displacement variation in time (upper frame) and the corresponding displacement level spectrum (lower frame). The displacement scale units in the upper frame are arbitrary and the time scale spans 78.1 ms.

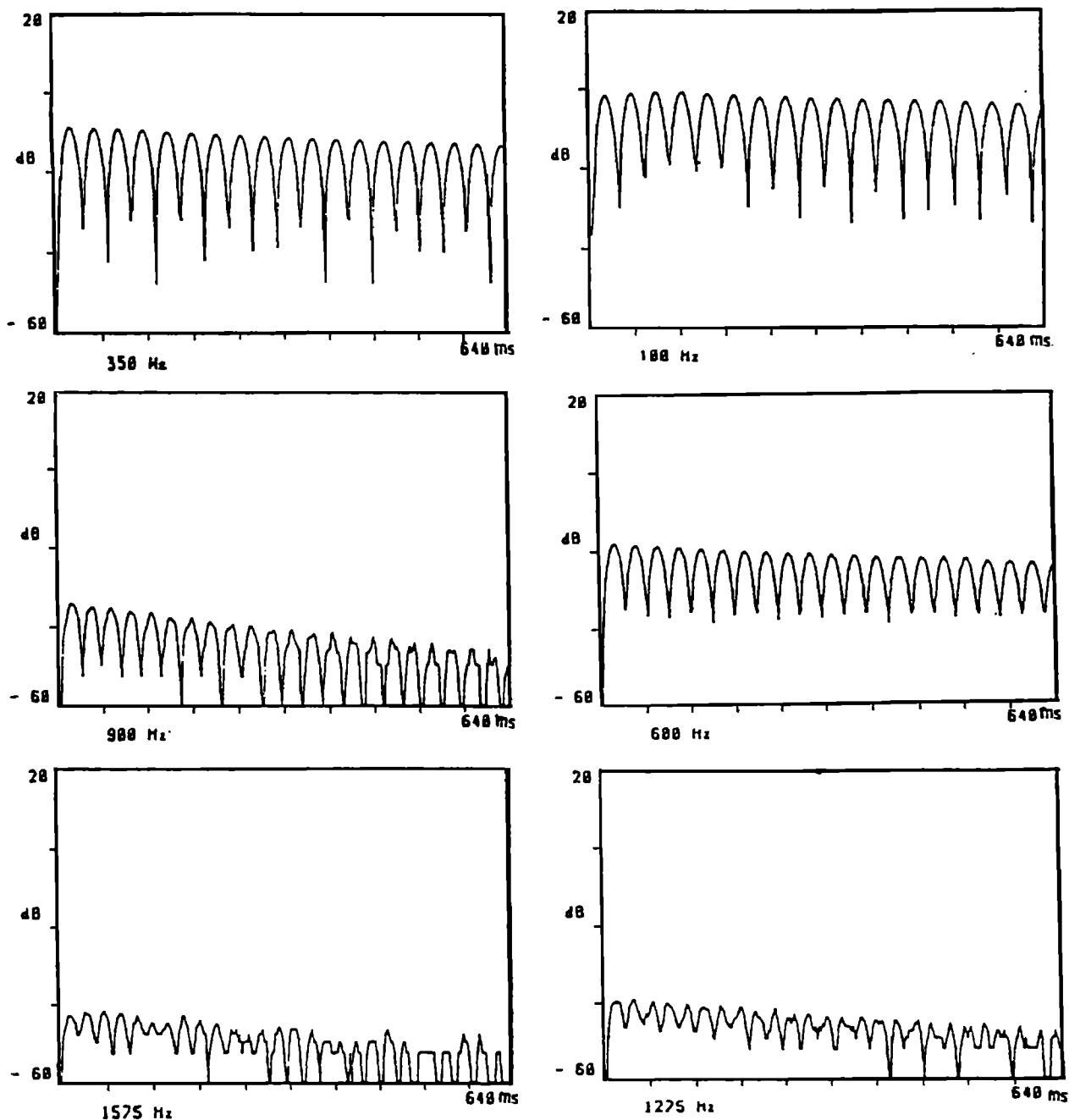


FIG. 5. Displacement level versus time plots of the  $A_0$  (27.5-Hz) string vibration. The center of each frequency channel is indicated below each frame. The time scales are synchronous and span 640 ms. The displacement level reference is arbitrary.

ratio. The signal levels in the plots at 900, 1275, and 1575 Hz in Fig. 5 were approaching the lower limit of the spectrum analyzer's 72-dB dynamic range, which corresponds to  $-52$  dB, relative to the maximum overall displacement level for the  $A_0$  signal.

On certain occasions (compare the 1575-Hz case in Figs. 5 and 6), the sound-signal analysis can yield a clearer pattern of periodic sound-pressure fluctuation under the same analysis conditions. This appears to be caused by an increase in the relative weighting of the sound-pressure levels in the high-frequency portion of the sound spectrum, resulting in a virtual expansion of the spectrum's dynamic range in this region. While a strong correlation existed between the changed frequency weighting of the sound-pres-

sure level and the position of the monitoring microphone, it is expected that other factors will contribute to this phenomenon, notably the transfer characteristics of the piano soundboard.<sup>15</sup> However, for reasons mentioned earlier, group velocity values obtained from sound-signal analysis should be used with caution.

The following parameters for the  $A_0$  string of the Yamaha G3 grand were adopted:  $\phi_s = 1.4 \times 10^{-3}$  m (steel core diameter);  $\phi_0 = 5.6 \times 10^{-3}$  m (overall  $A_0$  string diameter);  $S = 1.54 \times 10^{-6}$  m<sup>2</sup> (cross-sectional area of steel core);  $L = 1.35$  m;  $\rho_s = 7.8 \times 10^3$  kg m<sup>-3</sup> (volume mass density of copper);  $Y = 1.95 \times 10^{11}$  N m<sup>-2</sup> (Young's modulus of elasticity for steel piano wire);  $T/\sigma = 5.442 \times 10^3$  m<sup>2</sup> s<sup>-2</sup> (the minimum phase velocity value squared, estimated from

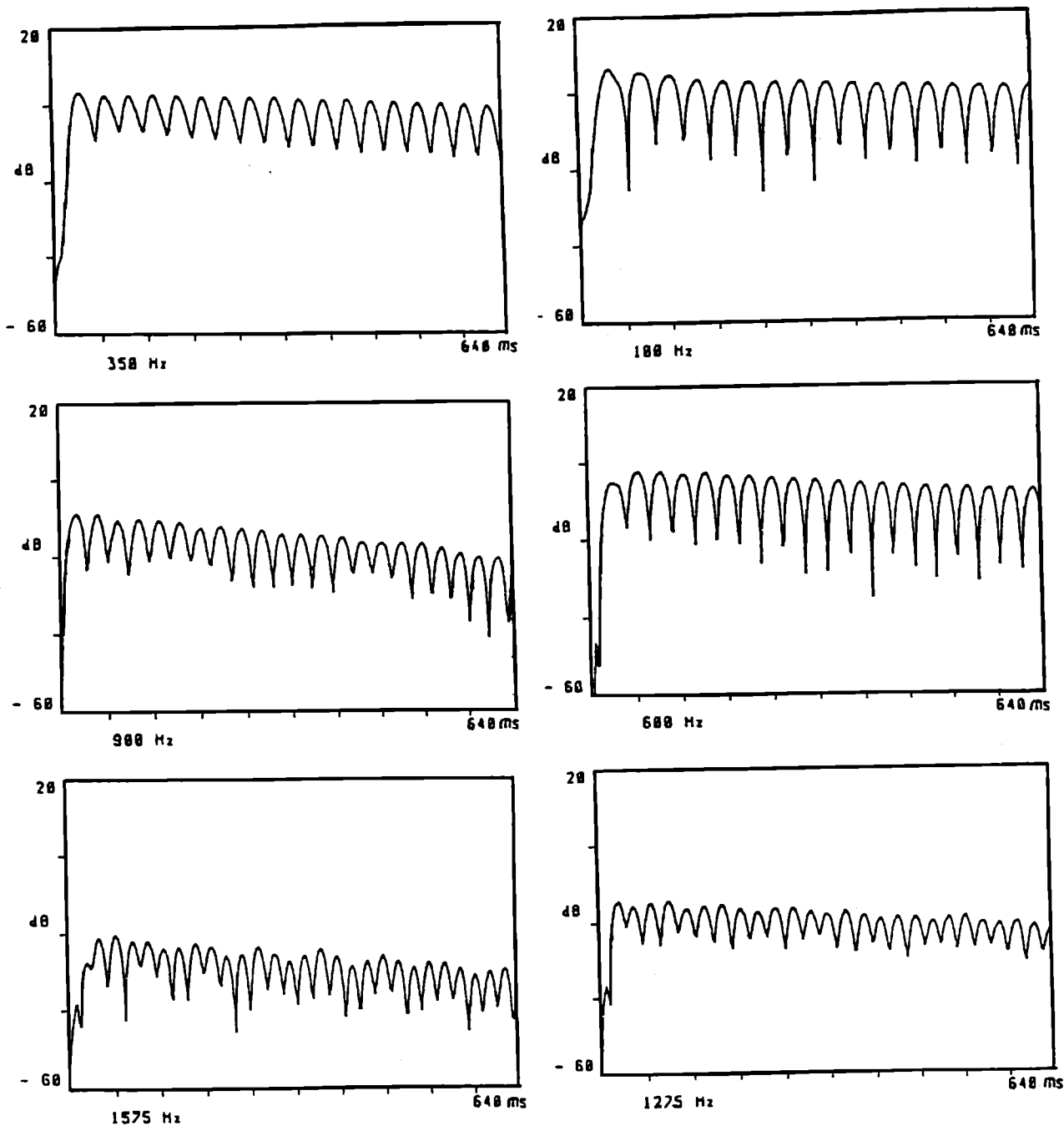


FIG. 6. Sound-pressure level versus time plots of the  $A_0$  (27.5-Hz) radiated sound corresponding to the string vibration plots in Fig. 5. The center of each frequency channel is indicated below each frame. The time scales are synchronous and span 640 ms. The sound-pressure level reference is arbitrary.

long-time frequency measurements of string vibration, where  $T/\sigma \approx (2L \times v_1)^2$ , with  $v_1 = 27.3$  Hz) and  $\sigma = 0.173$  kg/m (the average linear mass density of the  $A_0$  string). The Appendix shows how the average linear mass density of a piano bass string may be calculated.

Table I and the graph in Fig. 7(a) provide a comparison between the experimental and the theoretically derived values of  $v_g(\nu)$  for the  $A_0$  string. The uncertainty of the values of  $v_g$  obtained through Eq. (6) is not expected to exceed the uncertainty of values associated with experimental measurements. Because of a limited number of measurements, the experimental uncertainty is based more on the worst possible case estimates rather than statistical analysis. Both Table I

and Fig. 7(a) indicate a reasonable agreement between the values of  $v_g$  obtained from our measurements and those predicted from the theoretical model of a stiff string.

These findings for group velocity are further corroborated by the measurement of phase velocity  $v_p(\nu)$ . The measurement of  $v_p(\nu)$  is based on a standard method, such as the one used by Young,<sup>4,5</sup> in which well-resolved eigenfrequencies  $\nu_n$  of string vibration are used to calculate the corresponding phase velocity  $v_p(\nu_n)$ , namely,

$$v_p(\nu_n) = \nu_n 2L / n. \quad (9)$$

The  $A_0$  phase velocities were calculated from direct frequency measurements by use of Eq. (9) and compared with the

TABLE I. Measured group velocity  $v'_g(\nu)$  for the  $A_0$ (27.5-Hz) string, calculated from the measured time per one round-trip journey  $T(\nu)$  for groups with central frequency  $\nu$  and bandwidth of 25 Hz; also, the theoretical group velocity  $v_g(\nu)$ .

$\nu$ (Hz)	$T(\nu)$ (ms)	$v'_g(\nu)$ (m/s)	$v_g(\nu)$ (m/s)
0	...	...	73.7
$25 \pm 12.5$	$36.6 \pm 0.2$	$73.8 \pm 0.4$	73.7
$100 \pm 12.5$	$36.3 \pm 0.2$	$74.4 \pm 0.4$	74.0
$350 \pm 12.5$	$34.0 \pm 0.8$	$79.5 \pm 2.0$	77.3
$600 \pm 12.5$	$31.0 \pm 0.8$	$87.1 \pm 2.0$	83.6
$900 \pm 12.5$	$28.4 \pm 1.2$	$94.9 \pm 4.0$	93.4
$1275 \pm 12.5$	$24.7 \pm 2.2$	$110. \pm 10.$	107.0
$1575 \pm 12.5$	$22.5 \pm 2.8$	$120. \pm 15.$	118.0
$2000 \pm 12.5$	$19.7 \pm 2.8$	$137. \pm 19.$	134.0
$2700 \pm 12.5$	$17.1 \pm 2.8$	$158. \pm 22.$	157.0

theoretical values from Eq. (5) in Table II. The theoretical, as well as experimental, data for  $v_p$  are plotted in Fig. 7(a), together with data for  $v_g$ . The more rapid increase of  $v_g$  with frequency, compared to  $v_p$ , is consistent with the relationship expressed by Eq. (4). Similarly to  $v_g$ , reasonable agreement also exists between the experimental and theoretical values of  $v_p$ . While deviations important from the view of piano tuning may be observed, they are not large enough to warrant special attention in this type of study.

In Fig. 7(b) and (c), graphs of group and phase velocities are shown for the  $A_1$  (55-Hz) and  $A_3$  (220-Hz) strings, respectively. Again, a reasonable agreement was found to exist between the theoretical and experimental values of  $v_g$  and  $v_p$ , although, with the  $A_3$  strings (which are members of the plain piano-string class), considerable difficulties with group velocity measurements were experienced since the dispersion effect is no longer as prominent in the  $A_3$  strings as it is in the lower bass strings. This is also illustrated by the diminished development of low-amplitude precursors in the time-domain plots of the  $A_1$  and  $A_3$  string vibration signals, as shown in Figs. 8 and 9. Table III lists the physical parameters of  $A_1$  and  $A_3$  strings and Tables IV–VII show theoretical and measured values of  $v_g$  and  $v_p$  for the  $A_1$  and  $A_3$  strings in a manner analogous to Tables I and II.

It should be noted that the additional contribution to bending stiffness due to copper windings has not been included in our theoretical calculations of group and phase velocities since, in the gravest possible case, i.e., for the highest measured partial of the  $A_0$  string, an order of magnitude difference in stiffness-related factor would result in a 5% deviation in the phase velocity and a 10% deviation in the group velocity. Percentage difference calculations between the theoretical and experimentally obtained values of  $v_p$  and  $v_g$  show a maximum of 2% and 4% in the case of the  $A_0$  string, which illustrates the sensibility of our assumption.

Nonetheless, the effective value of the stiffness factor for piano bass strings can be obtained from the plots of inharmonicity factor versus mode number squared (see, for example, Refs. 4 and 5). By expressing inharmonicity  $\delta$  in cents as  $\delta = bn^2$ , where  $n$  is the mode number and  $b$  is the basic coefficient of inharmonicity,<sup>4</sup> we find that  $b$  depends on string

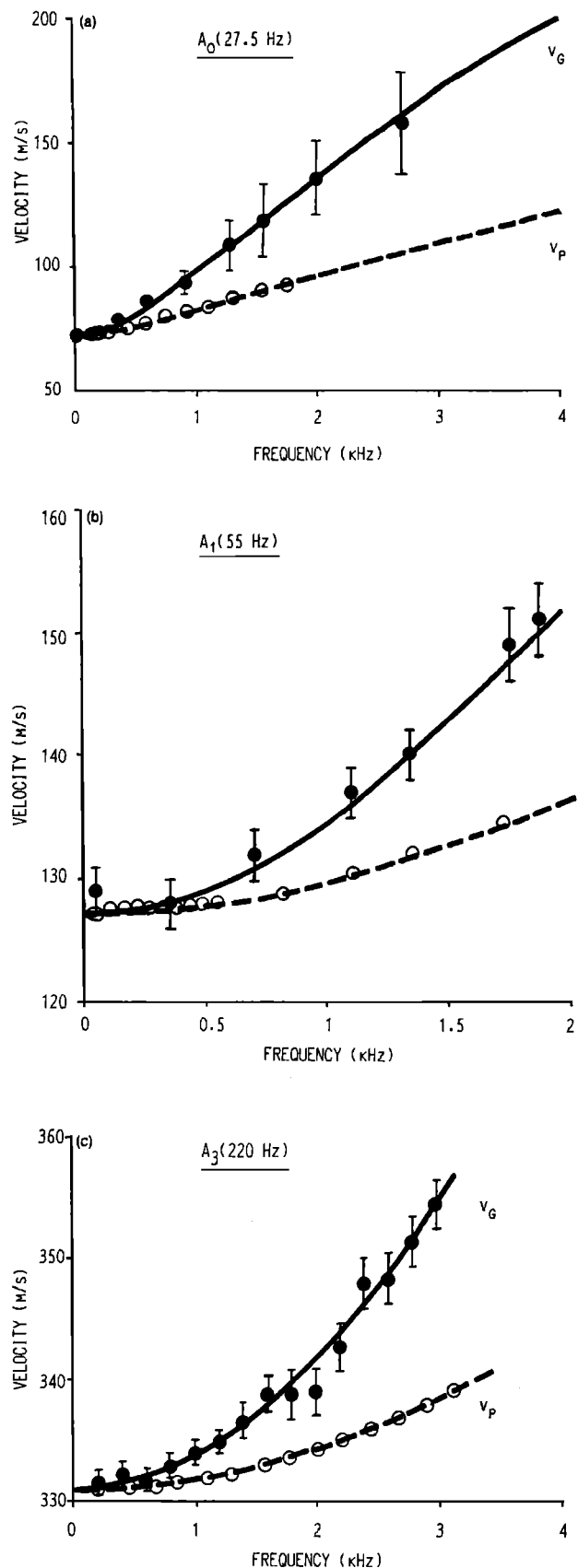


FIG. 7. Graphs of group and phase velocity versus frequency for the following three strings in the Yamaha G3 grand piano: (a) the  $A_0$  (27.5-Hz) string; (b) an  $A_1$  (55-Hz) string, and (c) an  $A_3$  (220-Hz) string. The continuous solid lines indicate the theoretical group velocities and the solid points with error bars represent the measured velocities. The broken lines correspond to theoretical phase velocity values, with the measured values indicated by circles.

TABLE II. Measured phase velocity  $v_p(\nu)$  calculated from the measured frequency  $\nu_n$  of the  $n$ th partial for the  $A_0$  (27.5-Hz) string; also, the theoretical phase velocity  $v_p(\nu)$ , with last three values of  $\nu_n$  chosen arbitrarily to illustrate general trend [see Fig. 7 (a)].

$n$	$\nu_n$ (Hz)	$v_p(\nu)$ (m/s)	$v_p(\nu)$ (m/s)
1	27.3	73.7	73.7
2	54.7	73.8	73.7
3	82.5	74.3	73.8
4	110.0	74.3	73.8
5	137.5	74.2	73.9
6	165.6	74.5	74.0
7	193.8	74.7	74.1
8	221.9	74.9	74.2
9	250.6	75.2	74.3
10	278.0	75.3	74.5
15	426.3	76.7	75.5
20	581.6	78.5	76.9
25	750.0	81.0	78.7
30	921.6	82.9	80.7
35	1108.	85.5	83.1
40	1306.	88.2	85.8
45	1521.	91.2	88.7
50	1748.	94.4	91.9
...	2400.	...	101.
...	3000.	...	109.
...	4000.	...	121.

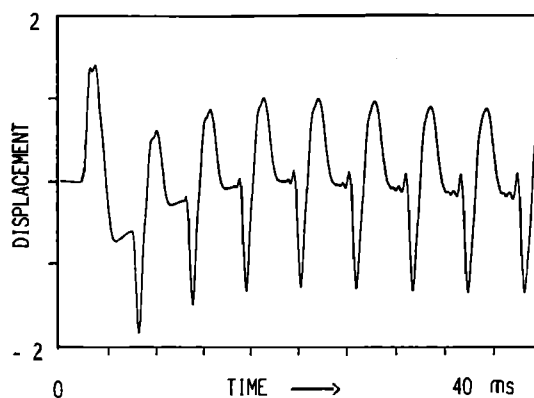


FIG. 9. A trace of the perpendicular-to-soundboard displacement of an  $A_3$  (220-Hz) string in time, showing the first eight initial pulses monitored near the agraffe end, on the opposite side of the bridge. The displacement scale unit is arbitrary.

tension, string length, diameter of steel core, and Young's modulus of elasticity. Since Young's modulus of elasticity is directly involved in determining inharmonicity in plain piano strings,<sup>4</sup> it is only natural that, in a simple model of a piano base string, its value could be suitably modified to account for the additional increase in inharmonicity due to the copper windings.

An estimate of the basic inharmonicity coefficient from the experimental data for the first ten modes of the  $A_0$  string is approximately 0.32 cents/ $n^2$ . This is about 70% higher than the value of 0.18 cents/ $n^2$  calculated according to the measured  $A_0$  string parameters with Young's modulus as that for the plain steel core, i.e.,  $Y = 1.95 \times 10^{11} \text{ N m}^{-2}$ . A similar comparison in the  $A_1$  string case yielded basic inharmonicity coefficients of 0.11 and 0.10 cents/ $n^2$ , respectively,



FIG. 8. A trace of the perpendicular-to-soundboard displacement of an  $A_1$  (55-Hz) string in time, showing the first four initial pulses monitored approximately 10 cm from the bridge. The unit of the displacement scale is arbitrary.

although this time the 15th and 20th mode frequencies were included in the experimental determination. As pointed out in Ref. 5, the inharmonicity values for the lower numbered modes in bass strings can deviate considerably from the linear pattern, when plotted against  $n^2$  and, therefore, some average value has to be established. In our examples, this was done through linear regression analysis.

In the theoretical calculations of group and phase velocities, we have conveniently retained the value of Young's modulus of elasticity as that for a plain string, since the additional inharmonicity generating factors, such as increased stiffness due to copper windings or impedance variation in string supports (e.g., Ref. 6, pp. 314–318), will not affect significantly our demonstration of the fundamental aspects of the phase and group velocity relation.

#### IV. DISCUSSION OF THE PHYSICAL EFFECTS OF DISPERSION ON THE ATTACK TRANSIENTS OF RADIATED SOUND

Besides group velocity measurement, one of our objectives in the study of dispersion of transverse waves in piano strings was to investigate whether it has any effect on the attack transients of the corresponding radiated sound. Benade (Ref. 6, p. 426) has alluded to dispersion effects in reference to the beginning of tones in brass wind instruments.

TABLE III.  $A_1$  (55-Hz) and  $A_3$  (110-Hz) string parameters, as defined for the  $A_0$  string.

Parameter	$A_1$ value	$A_3$ value	Units
$\phi_s$	$1.1 \times 10^{-3}$	$1.04 \times 10^{-3}$	m
$\phi_0$	$3.0 \times 10^{-3}$	$1.04 \times 10^{-3}$	m
$S$	$9.5 \times 10^{-7}$	$8.49 \times 10^{-7}$	$\text{m}^2$
$S_0$	$7.07 \times 10^{-6}$	$8.49 \times 10^{-7}$	$\text{m}^2$
$L$	1.175	0.756	m
$\rho_s$	$7.8 \times 10^3$	$7.8 \times 10^3$	$\text{kg m}^{-3}$
$\rho_c$	$8.9 \times 10^3$	$8.9 \times 10^3$	$\text{kg m}^{-3}$
$Y$	$1.95 \times 10^{11}$	$1.95 \times 10^{11}$	$\text{N m}^{-2}$
$T/\sigma$	$1.64 \times 10^4$	$1.10 \times 10^5$	$\text{m}^2 \text{ s}^{-2}$
$\nu_1$	54.13	219.0	Hz
$\sigma$	$5.024 \times 10^{-2}$	$6.63 \times 10^{-3}$	$\text{kg m}^{-1}$

TABLE IV. Measured group velocity  $v'_g(\nu)$  for one  $A_1$  (55-Hz) string, calculated from the measured time per one round-trip journey for groups with central frequency  $\nu$  and bandwidth of 50 Hz; also, the theoretical group velocity  $v_g(\nu)$ .

$\nu$ [Hz]	$v'_g(\nu)$ (m/s)	$v_g(\nu)$ (m/s)
50 ± 25	129 ± 2	127
350 ± 25	128 ± 2	128
700 ± 25	132 ± 2	131
1100 ± 25	137 ± 2	136
1350 ± 25	140 ± 2	141
1750 ± 25	149 ± 3	148
1850 ± 25	151 ± 3	150

Two examples of attack transients in the string vibration and the corresponding radiated sound are given in Figs. 10 and 11. Figures 10 and 11 show the temporal development of spectra of the string's time-differentiated displacement amplitude and of the corresponding sound-pressure amplitude for the  $A_0$  and  $A_1$  tones, respectively. In these figures, the plot at each time segment possesses its own vertical amplitude axis. Also, the application of the time differentiating function serves no purpose other than to highlight the higher frequency portions of the string displacement spectra through the introduction of a  $2\pi\nu$  factor.

A preliminary inspection of Figs. 10 and 11 reveals immediately two interesting features. First, the distinct, quasi-regular frequency glides, observed in the string vibration spectra, but not so clearly in those of the corresponding sound spectra, and second, the emergence of high-frequency components present in the attack portion of the radiated sound, which precede any development in the transverse string vibration spectra. This second feature is corroborated by Figs. 12 and 13, which illustrate the synchronized time traces of the  $A_0$  and  $A_1$  string displacement signal (monitored about 10 cm from the bridge) and those of sound pres-

TABLE V. Measured phase velocity  $v'_p(\nu)$  calculated from the measured frequency  $\nu_n$  of the  $n$ th partial for one  $A_1$  (55-Hz) string; also, the theoretical phase velocity  $v_p(\nu)$ .

$n$	$\nu_n$ (Hz)	$v'_p(\nu)$ (m/s)	$v_p(\nu)$ (m/s)
1	54.13	127.2	127.2
2	108.7	127.7	127.2
3	163.0	127.7	127.3
4	217.7	127.9	127.3
5	271.8	127.7	127.4
6	326.1	127.7	127.5
7	380.5	127.7	127.6
8	434.9	127.8	127.7
9	489.5	127.8	127.8
10	545.0	128.1	128.0
15	822.7	128.9	128.9
20	1110.	130.5	130.3
24 <sup>a</sup>	1350.	132.2	131.7
30	1718.	134.5	134.1

<sup>a</sup> The 25th partial was suppressed.

TABLE VI. Measured group velocity  $v'_g(\nu)$  for one  $A_3$  (220-Hz) string, calculated from the measured time per one round-trip journey for groups with central frequency  $\nu$  and bandwidth of 200 Hz; also, the theoretical group velocity  $v_g(\nu)$ .

$\nu$ (Hz)	$v'_g(\nu)$ (m/s)	$v_g(\nu)$ (m/s)
0 ± 100	...	331
200 ± 100	332 ± 1	331
400 ± 100	332 ± 1	332
600 ± 100	332 ± 1	332
800 ± 100	333 ± 1	333
1000 ± 100	334 ± 1	334
1200 ± 100	335 ± 1	335
1400 ± 100	336 ± 1	336
1600 ± 100	339 ± 1	338
1800 ± 100	339 ± 2	340
2000 ± 100	339 ± 2	342
2200 ± 100	343 ± 2	344
2400 ± 100	348 ± 2	346
2600 ± 100	348 ± 2	349
2800 ± 100	351 ± 2	352
3000 ± 100	354 ± 2	354

sure of the corresponding radiated sound (monitored about 10 cm above the central region of the soundboard). In both figures, it can be clearly seen that low-amplitude sound-pressure components emerge several milliseconds before the initial string displacement pulse is registered at the bridge.

In view of the apparent cause and effect conflict, we looked for an alternative mechanism, other than transverse string vibration, which could account for the generation of the observed precursive sound-pressure components. A short-time spectral analysis of the precursive sound-pressure components revealed a set of harmonically related peaks that could be related to the eigenfrequencies of the respective longitudinal string vibration. This is illustrated in Figs. 14-17.

The time trace of the precursive sound-pressure component for the  $A_0$  sound, together with its frequency spectrum,

TABLE VII. Measured phase velocity  $v'_p(\nu)$  calculated from the measured frequency  $\nu_n$  of the  $n$ th partial for one  $A_3$  (220-Hz) string; also the theoretical phase velocity  $v_p(\nu)$ .

$n$	$\nu_n$ (Hz)	$v'_p(\nu)$ (m/s)	$v_p(\nu)$ (m/s)
1	218.8	330.8	330.8
2	437.5	330.8	330.9
3	657.0	331.1	331.2
4	876.6	331.4	331.5
5	1098.	332.0	331.9
6	1320.	332.6	332.3
7	1542.	333.1	332.8
8	1765.	333.6	333.6
9	1990.	334.3	334.3
10	2215.	335.0	335.1
11	2444.	335.9	336.0
12	2673.	336.9	337.0
13	2905.	337.8	338.1
14	3141.	339.2	339.3

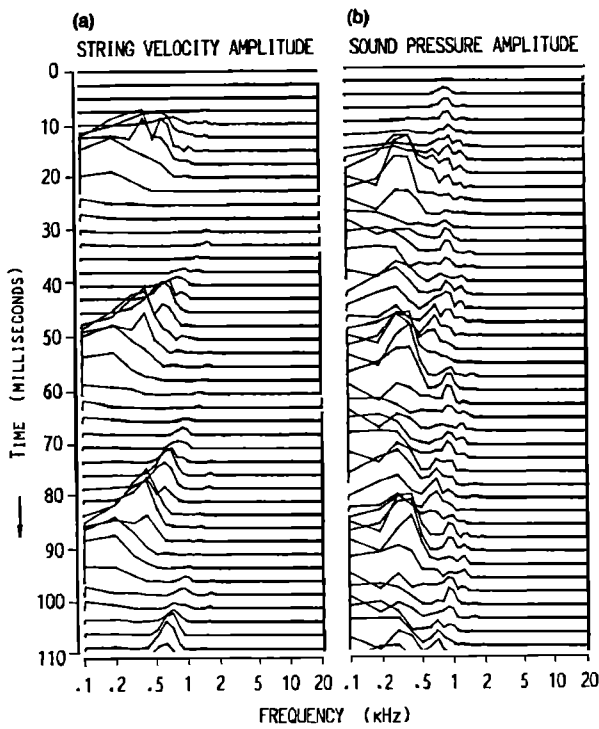


FIG. 10. (a) The temporal development of the  $A_0$  (27.5-Hz) spectrum of the time-differentiated string displacement signal. Each time segment has an implied vertical axis that effectively represents string velocity amplitude with an arbitrary unit. (b) The temporal development of the  $A_0$  (27.5-Hz) spectrum of the sound-pressure signal corresponding to (a). The implied vertical axis of each time segment denotes sound-pressure amplitude.

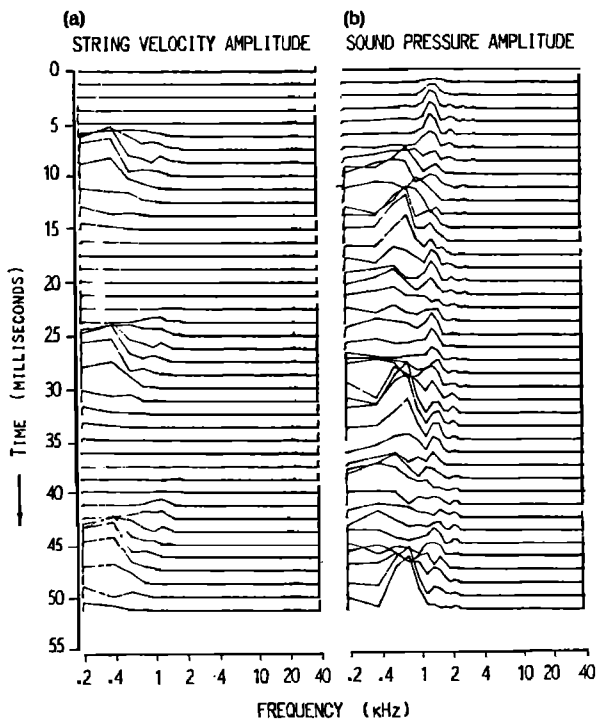


FIG. 11. (a) Temporal development of the  $A_1$  (55-Hz) spectrum of the time-differentiated string displacement signal. (b) Temporal development of the  $A_1$  (55-Hz) spectrum of the sound-pressure signal corresponding to (a). The plots in (a) and (b) are analogous to those in Fig. 10.

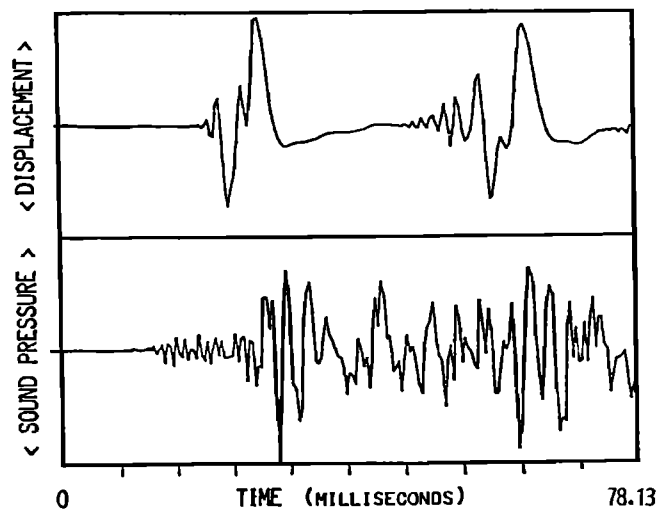


FIG. 12. Time-domain plots of the initial string displacement (upper frame) and sound pressure (lower frame) after striking of the  $A_0$  (27.5-Hz) key on the piano. The time scales in the upper and lower frames are synchronized, and the vertical scale units are arbitrary.

is shown in Fig. 14. Here, the sampling rate is 12.8 kHz and the windowing function is set to the rectangular option in order to display a well-defined spectrum free of transverse modes of string vibration. In Fig. 14(a), the time trace is approximately divided into the precursive sound portion (lower frame) and the continuing trace (upper frame), which includes sound-pressure components due to the transverse string vibration modes. Figure 14(b) represents the sound-pressure level spectrum of the lower frame in Fig. 14(a), with the harmonic cursor set to integral multiples of 475.0 Hz.

Figure 15 shows the spectrum of the  $A_0$  sound-pressure signal, when only longitudinal string modes are excited by stroking the string with a rosin coated cello bow in the string's longitudinal direction. The correspondence between

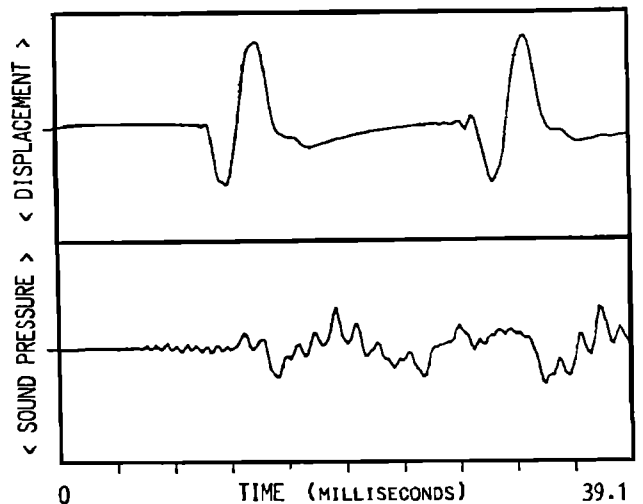


FIG. 13. Time-domain plots of the initial string displacement (upper frame) and sound pressure (lower frame) after striking of the  $A_1$  (55-Hz) key on the piano. The time scales in the upper and lower frames are synchronized and the vertical scale units are arbitrary.

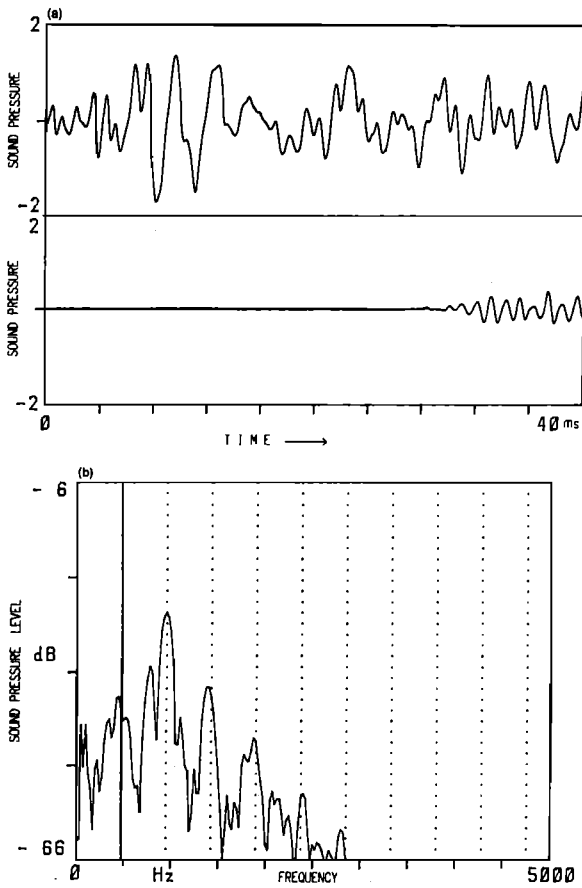


FIG. 14. (a) A plot of the initial  $A_0$  (27.5-Hz) sound-pressure variation in time. The trace begins in the lower frame and continues in the upper frame. The initial portion of the trace was deliberately sectioned off in the lower frame to delineate the "precursive sound" portion. The vertical scale units are arbitrary. (b) The spectrum of the precursive sound-pressure signal in (a). The harmonic cursor is set at integral multiples of 475 Hz with the main cursor set at the first harmonic, 475.0 Hz.

the harmonically related peaks of the two spectral distributions in Figs. 14 and 15 indicate a strong likelihood of  $A_0$  precursive sound being of longitudinal string vibration origin.

Similarly, Fig. 16(a) shows the time trace and Fig.

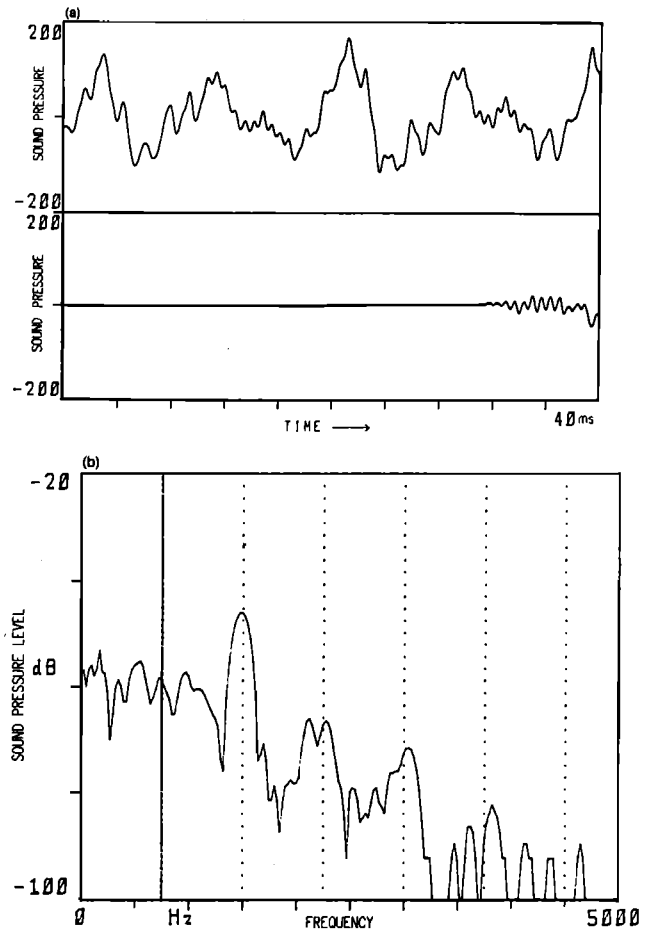


FIG. 16. (a) A plot of the initial  $A_1$  (55-Hz) sound-pressure variation in time, analogous to Fig. 14, where the lower frame delineates the "precursive sound" portion. (b) The spectrum of the precursive sound-pressure signal in (a). The harmonic cursor is set at integral multiples of 750 Hz and the main cursor is set at the first harmonic, 750.0 Hz.

16(b) the corresponding spectrum of the  $A_1$  precursive sound-pressure component; Fig. 17 shows the spectrum of the radiated sound when only longitudinal string modes are excited. The harmonic cursor in Figs. 16(b) and 17 is set to integral multiples of 750.0 Hz. Again, correspondence is found between the harmonically related peaks in both spec-

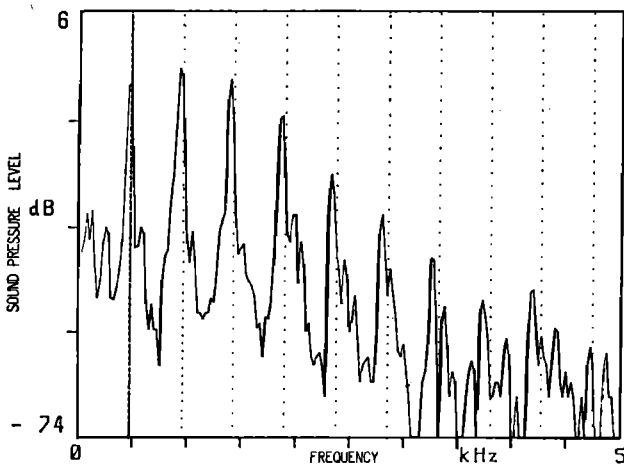


FIG. 15. The spectrum of the sound-pressure signal obtained by excitation of the longitudinal modes in the  $A_0$  (27.5-Hz) string. The harmonic cursor is set to the fundamental frequency of 475.0 Hz.

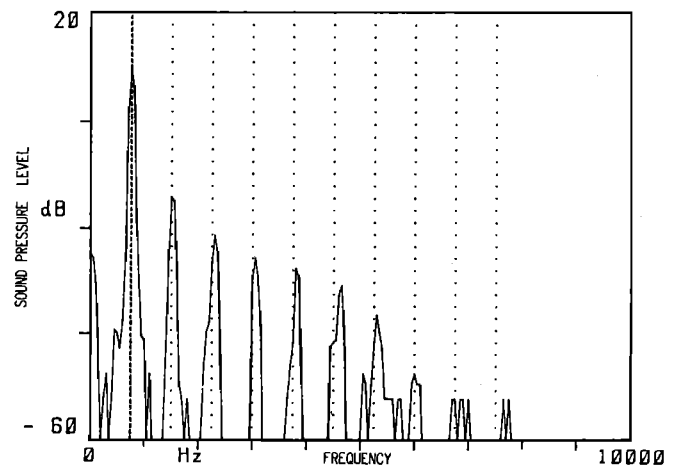


FIG. 17. The spectrum of the sound-pressure signal obtained by excitation of the longitudinal modes in the  $A_1$  (55-Hz) strings. The harmonic cursor is set to the fundamental frequency of 750.0 Hz.

tral distributions.

Without entering into a detailed discussion, it may be noted that the longitudinal mode frequencies in the  $A_0$  and  $A_1$  cases can be shown to correspond quite well to the longitudinal mode frequencies calculated according to the model of a simple uniform string, mounted between two rigid, massive supports.

A closer examination of the high-frequency onset in the time-differentiated sound-pressure spectra portrayed in Figs. 10(b) and 11(b) indicates that the precursive sound precedes the onset of sound originating from transverse string vibrations by approximately 12.5 and 7.5 ms, for  $A_0$  and  $A_1$  tones, respectively. For a given frequency band (with center frequency in the 1-kHz region for  $A_0$ , and in the 1.5-kHz region for  $A_1$ ), calculations of group velocities for longitudinal and transverse waves on the string revealed that the time delay between the two onsets can be almost entirely attributed to the time of travel of the transverse wave group from the hammer-impact point to the bridge. In both instances, the group velocity of longitudinal waves is more than an order of magnitude larger than the group velocity of the respective transverse waves.

Comparing our findings with those of Weyer,<sup>15,16</sup> we find that, in his study of attack transients of piano and harpsichord sounds, he has observed the presence of "restrained phenomenon of vibration," which has, as he claims, a more marked effect on the "tone rise" in the piano rather than the harpsichord. It appears that Weyer's observations relate, at least in part, to the precursive sound observed in our investigations, although no detailed analysis was given. He suggested a combination of plausible causes to explain the observed "restrained phenomenon of vibration," but did not include the possibility of a longitudinal string vibration mechanism, presumably because his study was limited to sound-pressure measurements only.

While the above examples of the  $A_0$  and  $A_1$  precursive sound analysis point to a correlation between the excitation of longitudinal modes in the string and precursive sound generation, a more detailed investigation of longitudinal modes of string vibration and their role in the attack transients of piano tones is the subject of another article. Thus the explanations offered here should be viewed only as indicative rather than substantive.

Because of the strong presence of components of longitudinal string vibration origin, we were unable to discern clearly the physical effect of dispersion of transverse waves in the string on the attack transients of the corresponding radiated sound. However, it is quite conceivable that the dispersion in low bass strings could affect considerably the psychoacoustic characteristics of the perceived attack transient of the radiated sound. An indication of such possibility is evident from listening to the tape recording of the transverse string displacement signal. It may be shown that, if the piano soundboard response were approximated to that of a simple piston, then the spectral distribution of the radiated sound pressure and its time development would essentially follow that of the string displacement, near the bridge support (see, for example, Ref. 2, p. 133, and Ref. 17).

It is also interesting to note that the observed effect of

dispersion of transverse waves in strings and the longitudinal mode excitation were most prominent in the piano's low bass register and decreased toward the treble.

## V. CONCLUSION

In this study, we were able to show, through several representative examples, that group velocity of transverse waves on piano strings may be measured with the use of a short-time spectral analysis technique. The results were essentially in agreement with predictions based on a model of a flexurally stiff string and consistent with the predicted relationship between phase and group velocity as functions of frequency. Naturally, such group velocity measurement methods can be extended to other situations besides the piano.

While the inharmonicity of piano tone partials represents a well-known effect of dispersion of transverse waves in strings, established through long-time spectral measurements, our study concentrated on the short-time effect. In particular, we wished to investigate the effect of dispersion on the attack transient of the radiated sound, related to transverse vibration of low bass strings. However, precursive sound-pressure components of longitudinal string vibration origin masked strongly the initial sound development, and the effect of dispersion on the attack transient of the radiated sound could not be established. Nonetheless, it is expected that further studies of the dispersion phenomenon will reveal its contribution to the attack transient of radiated sound.

## APPENDIX: LINEAR MASS DENSITY CALCULATIONS FOR PIANO BASS STRINGS

All bass strings on the Yamaha G3 grand piano have one or two layers of copper windings wrapped around a steel core. This method of increasing a bass string's linear mass density is, in fact, common to most modern brands of pianos. Most bass strings have a single winding of copper wire, and it is usually within the last octave that double winding is used.

A double-wound string consists of a bare steel core wrapped with a small diameter copper wire, which is then overspun with a larger diameter copper wire, covering the first layer as well as a small part of the steel core near the ends of the string. Thus only the outer winding is visible and the existence of the inner winding is evident only from the small change in the diameter of the overall covering near the ends.

When calculating the linear mass density of a bass string, we can approximate the string composition to a thin cylinder of steel surrounded by either one or two layers of copper toroids, rather than helices. In the case of a double-wound string, it is expected that both the inner and outer windings will have the kind of packing efficiency as that for a helix wound on a smooth cylinder, since the difference in wire diameters for the inner and outer windings is usually quite large. In the Yamaha  $A_0$  string, the ratio of the diameters of the inner and outer winding is approximately 3:1.

Thus, for a steel core of diameter  $\phi_s$  with volume density  $\rho_s$  and two copper windings with volume mass density  $\rho_c$  and wire diameters  $\phi_i$  and  $\phi_o$ , respectively, one can apply the

toroidal approximation to calculate the average linear mass density of the string  $\sigma$  as follows<sup>18</sup>:

$$\sigma = \rho_s \pi \phi_s^2 / 4 + \rho_c \pi^2 [\phi_s (\phi_i + \phi_o) + (\phi_i + \phi_o)^2] / 4. \quad (\text{A1})$$

Equation (A1) is applicable<sup>18</sup> to single, as well as double-wound strings. In the case of the Yamaha A<sub>0</sub> string,  $\phi_i \approx 5.0 \times 10^{-4}$  m,  $\phi_o \approx 1.6 \times 10^{-3}$  m, resulting in  $\sigma \approx 0.173$  kg m<sup>-1</sup>.

## ACKNOWLEDGMENTS

The authors wish to thank the Australian Research Grants Committee for the support of this project and Dr. R. W. Young for his valuable comments and criticism.

<sup>1</sup>Lord Rayleigh (J. W. Strutt), *The Theory of Sound* (Dover, New York, 1945), Vol. I, p. 296.

<sup>2</sup>P. M. Morse, *Vibration and Sound* (McGraw-Hill, New York, 1948), 2nd. ed.

<sup>3</sup>H. Fletcher, "Normal vibration frequencies of a still piano string," *J. Acoust. Soc. Am.* **36**, 203–209 (1964).

<sup>4</sup>R. W. Young, "Inharmonicity of plain wire piano strings," *J. Acoust. Soc. Am.* **24**, 267–273 (1952).

<sup>5</sup>R. W. Young, "Inharmonicity of piano strings," *Acustica* **4**, 259–262 (1954).

<sup>6</sup>A. H. Benade, *Fundamentals of Musical Acoustics* (Oxford U. P. New York, 1976).

<sup>7</sup>G. R. Baldock and T. Bridgeman, *The Mathematical Theory of Wave Motion* (Horwood, Chichester, England 1981).

<sup>8</sup>R. Johns, "Musical string vibrations," *Phys. Teacher* **15**, 145–156 (1977).

<sup>9</sup>M. Podlesak and A. R. Lee, "A photovoltaic detector for string vibration measurement," *J. Acoust. Soc. Am.* **79**, 2092–2093 (1986).

<sup>10</sup>G. Weinreich, "Coupled piano strings," *J. Acoust. Soc. Am.* **62**, 1474–1484 (1977).

<sup>11</sup>G. Weinreich, "The coupled motions of piano strings," *Sci. Am.* **240**, 94–102 (1979).

<sup>12</sup>E. Metzger, "Analysis of musical sounds by Fourier transform methods," *J. Acoust. Soc. Am.* **42**, 896–897 (1967).

<sup>13</sup>R. J. Alfredson and S. Steinke, "Fourier transform methods for analysing the sounds of a piano," *Acustica* **39**, 130–132 (1978).

<sup>14</sup>C. A. Coulson, *Waves* (Oliver and Boyd, Edinburgh, 1960), 7th ed., Chap. 8, pp. 128–138.

<sup>15</sup>R. D. Weyer, "Time-frequency-structures in the attack transients of piano and harpsichord sounds—I," *Acustica* **35**, 232–252 (1976).

<sup>16</sup>R. D. Weyer, "Time-varying amplitude-frequency-structure in the attack transients of piano and harpsichord sounds—II," *Acustica* **36**, 241–258 (1976/77).

<sup>17</sup>N. H. Fletcher, "Analysis of the design and performance of harpsichords," *Acustica* **37**, 139–147 (1977).

<sup>18</sup>R. W. Young, private communication (March 1987).